
Temporal Triplane Transformers as Occupancy World Models

Haoran Xu^{1,2}, Peixi Peng^{2,3†}, Guang Tan^{1†}, Yiqian Chang^{2,4}, Yisen Zhao³, and Yonghong Tian^{2,3,5}

¹ School of Intelligent Systems Engineering, Shenzhen Campus of Sun Yat-sen University, Shenzhen 518107, China.

² Peng Cheng Laboratory, Shenzhen 518108, China.

³ School of Electronic and Computer Engineering, Shenzhen Graduate School, Peking University, 518066, China.

⁴ School of Computer Science and Technology, Harbin Institute of Technology, Shenzhen, 518055, China.

⁵ School of Computer Science, Peking University, Beijing 100871, China.

ABSTRACT

Recent years have seen significant advances in world models, which primarily focus on learning fine-grained correlations between an agent’s motion trajectory and the resulting changes in its surrounding environment. However, existing methods often struggle to capture such fine-grained correlations and achieve real-time predictions. To address this, we propose a new 4D occupancy world model for autonomous driving, termed T³Former. T³Former begins by pre-training a compact triplane representation that efficiently compresses the 3D semantically occupied environment. Next, T³Former extracts multi-scale temporal motion features from the historical triplane and employs an autoregressive approach to iteratively predict the next triplane changes. Finally, T³Former combines the triplane changes with the previous ones to decode them into future occupancy results and ego-motion trajectories. Experimental results demonstrate the superiority of T³Former, achieving 1.44× faster inference speed (26 FPS), while improving the mean IoU to 36.09 and reducing the mean absolute planning error to 1.0 meters.

Keywords Occupancy world models · Triplane · Multi-scale · Autoregression

1 Introduction

World models [1, 2] are designed to predict future scenes and facilitate motion planning for agents. These models first construct lower-dimensional representations of the scenes, which serve as a foundation for learning the patterns of environmental dynamics. This capability supports the identification of potential dangers, the determination of traffic participants’ intentions, and ultimately leads to improved decision-making.

This paper focuses on world models for autonomous driving [3, 4, 5, 6, 7], where accurately predicting the future behavior of traffic participants is essential for the agent’s planning. Existing methods [8, 6, 7, 9] mainly provide instance-level predictions for traffic participants from a Bird’s Eye View (BEV) perspective, or directly utilize diffusion models [10, 11, 12, 13, 14] to generate future pixel-level driving views. However, these methods have difficulty in establishing fine-grained, 3D associations between changes in the scene and the agent’s motion planning. Recent advancements in 3D occupancy technologies [15, 16, 17, 18, 19] have gained significant attention from both academia and industry [20, 21]. 3D occupancy offers a well structured 3D representations of surroundings, which facilitates motion planning by establishing fine-grained correlations between surrounding occupied voxels and the agent’s actions.

In this context, the first task is to learn a compact, lower-dimensional representation of the raw occupancy data [4, 3, 5], which must preserve both geometric and semantic details. Current methods mainly employ VQ-VAE [22] for the purpose. While VQ-VAE has shown success in several generative tasks [23, 24, 25], its application to compressing occupancy data forces the latent space of 3D structures to be discretized. This results in different 3D structures sharing the same token in the codebook, inevitably causing a loss of 3D structural features and reduced reconstruction accuracy. Furthermore, in real-world scenarios, most voxels in the occupancy data are empty (unoccupied) [26], and some objects

[†]Corresponding authors

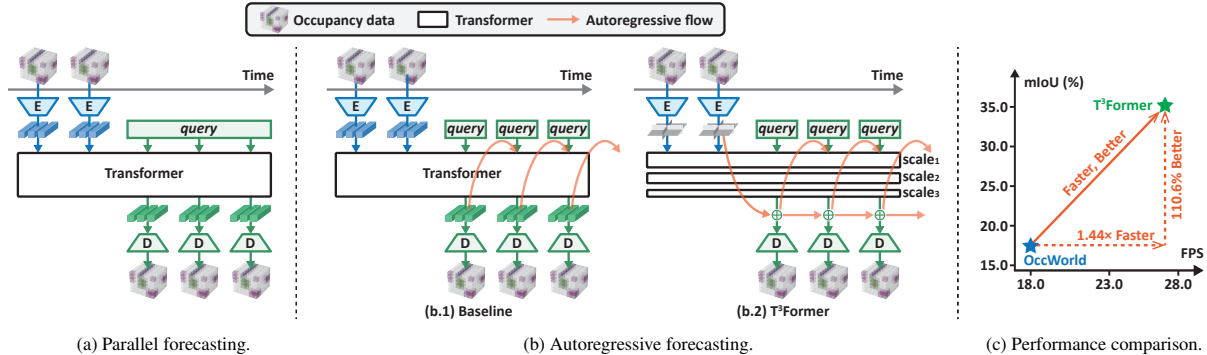


Figure 1: Different principles of occupancy world models: (a) **Parallel forecasting** [4, 5], which inputs all future queries and historical occupancy results, using a Transformer [27] architecture to predict future occupancy results in parallel; and (b) **Autoregressive forecasting** [3], which predicts future results iteratively, conditioning each step on a single future query and the previous frame’s prediction. Existing models typically use pre-trained VQ-VAE [22] to compress occupancy results into a compact representative code for predicting future codes. In contrast, our T³Former, shown in (b.2), employs more precise and efficient triplane representations and leverages multi-scale Transformers to predict triplane changes. Therefore, we achieve faster and more accurate occupancy forecasting, as shown in (c).

contain only a small number of semantic voxels (e.g., pedestrians, road signs). This leads to the omission of sparse but critical details in the compressed features.

Based on the scene representation, recent world models [5, 4] often employ Transformers for future state prediction. A key challenge for these approaches is capturing the diverse motion patterns of multi-scale objects on the road. For example, small objects like pedestrians or bicycles may exhibit sudden and abrupt motion changes, while larger objects such as trucks or buses tend to demonstrate more inertial movement, potentially requiring a different modeling granularity. Furthermore, they employ the Transformer to directly predict the *complete future occupancy state*. This end-to-end approach requires the model to learn both state changes and absolute state reconstruction simultaneously, increasing the learning burden. This not only demands larger model capacity but also increases the risk of error accumulation in long-term predictions.

We present a novel occupancy world model using *temporal triplane transformers* (T³Former) that addresses the aforementioned challenges. First, we propose to compress the 3D occupancy data into a *triplane* structure, a concept from computer graphics [28, 29, 30, 31, 32, 33]. A triplane comprises three planes – xy , xz , and yz – onto which the occupancy data are projected. Compared to VQ-VAE, this representation ensures high reconstruction accuracy of the occupancy grid, achieving a 20% improvement in mIoU while reducing the latent space size by 34%. Next, we extend the representation to the temporal dimension (xyt , xzt , and yzt), using Transformer models across multiple scales to regressively generate incremental changes in the triplane. Finally, we leverage these changes, along with the previous occupancy state, to predict future occupancy and perform motion planning.

Compared to OccWorld, T³Former reduces the total model size by 23%, while also mitigating the cumulative error in long-term occupancy predictions, resulting in a 110.6% increase in mIoU. At the same time, the motion planning accuracy achieves the lowest average error of 1.0 meters and the lowest average collision rate of 30%. This is mainly because we focus on predicting multi-scale occupancy state changes within the triplane space, which more effectively capture environmental dynamics. In summary, our contributions are mainly three-fold:

- We design a new 4D autoregressive occupancy world model, T³Former, that enhances long-term scene forecasting and enables precise motion planning.
- T³Former pre-trains a compact occupancy triplane representation to predict future incremental changes of triplanes using multi-scale Transformers. These changes, combined with the previous frame’s output, are then decoded into occupancy states and motion trajectories.
- Extensive experiments validate our state-of-the-art (SOTA) performance in terms of occupancy forecasting, motion planning, and real-time execution.

2 Related Works

3D occupancy reconstruction. 3D occupancy reconstruction techniques [15, 16, 17, 18, 19, 34] primarily utilize multi-camera RGB images or LiDAR point clouds as inputs to reconstruct the surrounding environment into an agent-centric 3D occupancy space, represented as fixed-size voxels. Each voxel contains a four-tuple attribute [15]: 3D coordinates (x , y , and z) and a semantic category. Existing methods mainly focus on how to establish precise semantic correlations between the raw sensor inputs and the 3D voxels. Once an accurate occupancy reconstruction is achieved, further learning of the temporal dynamics of scene changes becomes necessary [35].

4D occupancy prediction. To infer potential future scene changes, extensive 4D occupancy prediction approaches have been developed to learn the underlying temporal dynamics of scene evolution. Some methods [36, 37, 38] aim to predict future sensor-level data, which is then voxelized into occupancy data, while others [21, 39, 40, 41] leverage historical observations to directly predict occupancy outcomes. These methods mainly focus on reducing spatio-temporal biases on future occupancy predictions. However, they overlook the use of predicted scenes for effective and comprehensive motion planning.

World models for autonomous driving. World models [1, 2] aim to compress high-dimensional scene representations to capture the temporal dynamics of scene transitions, facilitating both future scene predictions and motion planning for the agent. In autonomous driving, existing models [8, 6, 7, 9] typically map surrounding traffic participants to the BEV perspective to predict instance-level tracklets or directly use diffusion models [10, 11, 12, 13, 14] to generate pixel-level future driving views. These methods derive control signals for the agent from current observations and predicted surroundings, but they rely solely on 2D BEV or image space, which limits the ability to establish fine-grained, efficient correlations between scene changes and motion planning. Recent world models [4, 5, 3] have leveraged 3D occupancy data to address this issue. However, they typically use VAE-series [22] models for environment compression, which often neglect original 3D geometric information and compromises reconstruction accuracy. Additionally, they rely on Transformers [27] to forecast the entire future scene instead of incremental changes, leading to significant error accumulation.

3 Methodology

3.1 Formulation

Next, we provide the formulation of Occupancy World Model (OWM) [3]. OWM primarily receives a sequence of scene representations and motion actions from past τ_p frames up to the current timestep t , such that $S^t \in \mathbb{R}^{H \times W \times L}$ represents the occupancy data of the agent-centric surrounding environment, with H , W , and L denoting the height, width, and length, respectively, and $a^t \in \mathbb{R}^2$ denotes a transition-related motion command. The goal of OWM is to establish a stochastic mapping, Φ , that associates past occupancy data and actions with future τ_f frames of occupancy data and action proposals. Formally:

$$S^{t:t+\tau_f}, a^{t:t+\tau_f} = \Phi(S^{t-\tau_p:t}, a^{t-\tau_p:t}). \quad (1)$$

To achieve this, we first pretrain a compressed latent representation of raw occupancy data using an Auto-encoder framework. The encoder and decoder models have parameters Φ_{enc} and Φ_{dec} , respectively. Thus, we have:

$$s^t = \Phi_{enc}(S^t), \quad \hat{S}^t = \Phi_{dec}(s^t). \quad (2)$$

where s^t and \hat{S}^t represent the latent representation and the corresponding reconstructed occupancy data, respectively.

Once we obtain the latent scene representations, we can predict future latent states with incremental changes Δs^{t+1} . These changes can be aggregated with the data from previous frames and decoded back into occupancy outcomes:

$$\Delta s^{t+1}, s^{t+1} = \Phi_{fut}(s^{t-\tau_p:t}), \hat{X}^{t+1} = \Phi_{dec}(s^{t+1}). \quad (3)$$

Next, we utilize the incremental latent changes, along with the latent states before the change, and the historical actions, to generate future transitions as follows:

$$a^{t+1} = \Phi_{act}(a^{t-\tau_p:t}, s^t, \Delta s^{t+1}). \quad (4)$$

Note that our OWM, $\Phi = \{\Phi_{enc}, \Phi_{dec}, \Phi_{fut}, \Phi_{act}\}$, operates in an autoregressive fashion. In particular, Equations (3) and (4) iteratively use previously predicted outcomes as part of the historical data to forecast future scenes and provide motion proposals.

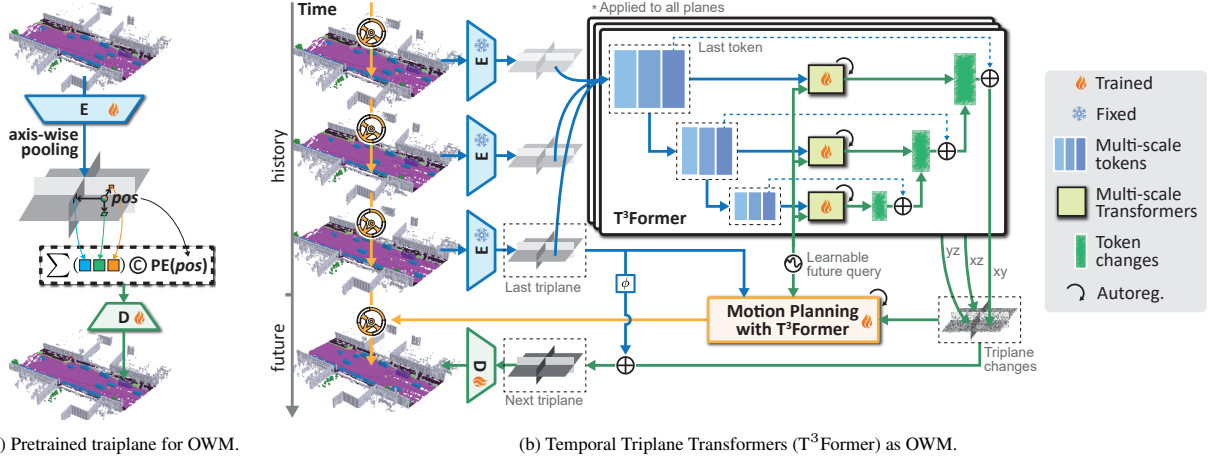


Figure 2: Workflow of T³Former. T³Former first pre-trains compact triplane representations of occupancy data. Next, T³Former utilizes multi-scale Transformers to capture comprehensive temporal dynamics within each plane, thereby predicting future changes in the triplane. Finally, T³Former leverages these predicted changes, along with the previous triplane, to generate future motion proposals.

3.2 T³Former as OWM

3.2.1 Pre-training triplane representations for OWM

To enable faster and more accurate predictions of future scenes $X^{t:t+\tau_f}$ by OWM, it is essential to compress the high-dimensional voxelized occupancy scene with high reconstruction accuracy. To achieve this, we employ the Triplane technique [33], which is widely used in volume rendering [28, 29, 30, 31, 32], to compress raw occupancy data in an orthogonal decomposition fashion.

Specifically, as shown in Figure 2a, the occupancy data S^t is first encoded by Φ_{enc} to produce $s^t \in \mathbb{R}^{C_s \times H_s \times W_s \times L_s}$. Then, an axis-wise average pooling operation is applied to obtain three orthogonal feature planes, $s^t = [s_{xy}^t, s_{xz}^t, s_{yz}^t]$, where $s_{xy}^t \in \mathbb{R}^{C_s \times W_s \times L_s}$, $s_{xz}^t \in \mathbb{R}^{C_s \times H_s \times W_s}$, and $s_{yz}^t \in \mathbb{R}^{C_s \times H_s \times L_s}$, corresponding to the xy , xz , and yz planes, respectively. To decode the original occupancy data, for each point in the 3D occupancy grid, denoted as $pos = (x, y, z)$, it serves as a position query to retrieve the corresponding features from the three planes in s^t . These features are then summed and concatenated with the positional encoding $\text{PE}(pos)$, which is passed into Φ_{dec} to predict the semantic label for the position pos . The detailed structures of Φ_{enc} and Φ_{dec} are given in the supplementary material.

By pretraining Φ_{enc} and Φ_{dec} with Equation (5), we obtain a highly generalizable and accurate triplane representation:

$$J_{\text{enc,dec}} = \mathbb{E}_{t \sim \mathcal{T}, pos \sim S^t} [\mathcal{L}_{\text{occ}}(\Phi_{\text{dec}}(\Phi_{\text{enc}}(S^t)), S^t)], \quad (5)$$

where \mathcal{T} represents the collection of all timesteps in the occupancy dataset, and $\mathcal{L}_{\text{occ}} = \mathcal{L}_{\text{ce}} + \lambda \mathcal{L}_{\text{lz}}$. Here, \mathcal{L}_{ce} and \mathcal{L}_{lz} denote the cross-entropy and Lovasz-softmax losses [42, 33], respectively, and λ is the trade-off factor.

The triplane representation, compared to the tokens generated by the VQ-VAE in OccWorld [3] and the MS-VAE in OccLLM [5], retains 3D structural information while achieving a more compact latent space. This not only makes our OWM more lightweight but also reduces the cumulative prediction error over time, as detailed later.

3.2.2 Multi-scale autoregressions in T³Former

Our T³Former model functions similarly to GPT-series [43, 44, 45], leveraging historical triplanes to generate future triplanes and using each predicted triplane to iteratively forecast subsequent ones. At timestep t , given the historical τ_p frames of triplanes $s^{t-\tau_p:t}$, the goal of T³Former is to capture the full temporal dynamics of the scene, particularly adapting to the motion patterns of objects of varying sizes. To achieve this, T³Former follows two key steps: (i) predicting each plane’s future changes, $\{\Delta s_i^{t:t+\tau_f} \mid i \in \{xy, xz, yz\}\}$, using Transformers with multiple scales; and (ii) aggregating these changes into the previous plane state and aligning the three plane predictions by fine-tuning the decoder Φ_{dec} .

In particular, $\Phi_{\text{fut}} = \{\Phi_{\text{fut}_{xy}}, \Phi_{\text{fut}_{xz}}, \Phi_{\text{fut}_{yz}}\}$. Each plane’s prediction model, Φ_{fut_i} , consists of Transformers [27] operating at multiple scales. These Transformers share the same architecture but have distinct learnable parameters and

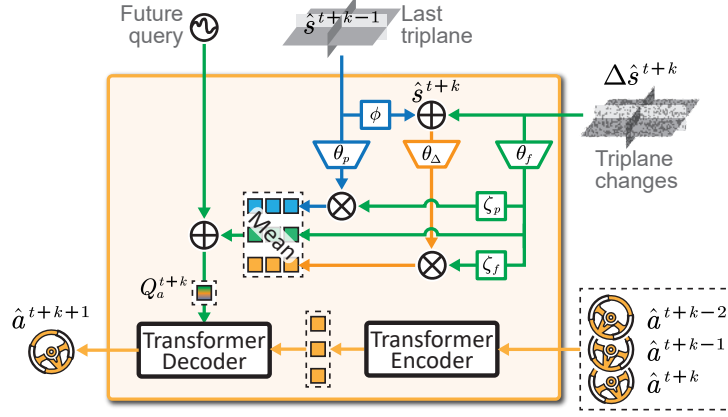


Figure 3: Motion planning with T³Former.

varying input sizes, depending on the plane and scale, as shown in Figure 2b. For example, in the case of $\Phi_{\text{fut},xy}$, the input s_{xy}^t is passed through UNet [46]-style downsampling, resulting in V scales of plane features. The feature at each scale $v \in V$ is denoted as $s_{xy}^{t,v} \in \mathbb{R}^{C_{s_{xy}}^v \times W_{s_{xy}}^v \times H_{s_{xy}}^v}$. These features are then flattened across the last two dimensions to form $W_{s_{xy}}^v \times H_{s_{xy}}^v$ tokens, which are input into the Transformer encoder to generate spatio-temporal memory. Next, we employ a learnable query $Q_{s_{xy}}^{t,v}$, which has the same dimension as $s_{xy}^{t,v}$, to enable cross-attention in the Transformer decoder and generate the token change from the current to the next time step based on the memory. Finally, the token changes at all scales are aggregated using UNet-style upsampling, yielding the plane’s feature change at the next time step, $\Delta \hat{s}_{xy}^{t+1}$. This change is then combined with the previous plane state, \hat{s}_{xy}^t , through a convolutional operation ϕ with a 1×1 kernel size.

The autoregressive forecasting process is given by:

$$\Delta \hat{s}_i^{t+k} = \Phi_{\text{fut}_i}(\hat{s}_i^{t+k-\tau_p:t+k}, Q_{s_i}^{t+k}), \quad (6)$$

$$\hat{s}_i^{t+k} = \Delta \hat{s}_i^{t+k} + \phi(\hat{s}_i^{t+k-1}), \quad (7)$$

$$\hat{S}^{t+k} = \Phi_{\text{dec}}(\hat{S}^{t+k} := \{\hat{s}_i^{t+k}\}), \quad (8)$$

where $i \in \{xy, xz, yz\}$, $k \in \{1, \dots, \tau_f\}$ is the timestep of autoregressive forecasting, and $Q_{s_i}^{t+k}$ is the learnable query at timestep $t+k$ in the i -th plane.

Since we have pre-trained the triplane occupancy representations, the future triplane can be used as the ground truth (GT) to supervise T³Former. Besides, we finetune Φ_{dec} to the separate predictions of each plane. Formally:

$$J_{\text{fut}} = \mathbb{E}_{t,k,i}[\mathcal{L}_{\text{fut}}(\hat{s}_i^{t+k}, s_i^{t+k}) + \xi \mathcal{L}_{\text{occ}}(\hat{S}^{t+k}, S^{t+k})], \quad (9)$$

where \mathcal{L}_{fut} is the weighted sum of L1 and L2 losses, defined as $\mathcal{L}_{\text{fut}} = \mathcal{L}_1 + \gamma \mathcal{L}_2$, and γ, ξ are trade-off weights.

3.3 Motion planning with T³Former

Given the predicted scene changes, $\Delta \hat{s}^{t+k}$, provided by T³Former, we can generate a comprehensive motion plan by anticipating potential dangers based on both the scene changes and the previous and next scenes.

To achieve this, we first map the previous frame triplane \hat{s}^{t+k-1} , the triplane change $\Delta \hat{s}^{t+k}$, and the next frame triplane \hat{s}^{t+k} through the ResNet-18 networks [47] θ_p , θ_Δ , and θ_f , respectively, into a shared latent space, denoted as z^{t+k-1} , Δz^{t+k} , and z^{t+k} . Then, Δz^{t+k} passes through two independent fully connected (FC) layers and Sigmoid layers, collectively referred to as ζ_p and ζ_f , to generate the query vectors f^{t+k-1} and f^{t+k} , which are then multiplied with z^{t+k-1} and z^{t+k} to obtain the motion-related features of the scene change relative to the last triplane and the next triplane. Finally, the motion-related features and the scene change Δz^{t+k} are element-wise averaged and processed through a FC layer, and then added to the future position encoding, resulting in the query variable for the next timestep motion plan, $Q_a^{t+k} \in \mathbb{R}^{d_{\text{act}}}$.

Next, we project the actions of the historical τ_p frames into the same dimension as Q_a^{t+k} , and employ a Transformer encoder to capture the motion dependencies within these frames. Then, Q_a^{t+k} is used in the Transformer decoder via

Models	Input	mIoU (%) \uparrow					IoU (%) \uparrow				
		0s	1s	2s	3s	Avg.	0s	1s	2s	3s	Avg.
Copy&Paste	3D-Occ	66.38	14.91	10.54	8.52	11.33	62.29	24.47	19.77	17.31	20.52
OccWorld-O [3]	3D-Occ	66.38	25.78	15.14	10.51	17.14	62.29	34.63	25.07	20.18	26.63
Vanilla-LLaMA-O [4]	3D-Occ	-	14.15	9.80	6.77	10.24	-	21.36	18.31	14.82	18.16
OccLLaMA-O [4]	3D-Occ	75.20	25.05	19.49	15.26	19.93	63.76	34.56	28.53	24.41	29.17
OccLLM-O [5]	3D-Occ	-	24.02	21.65	17.29	20.99	-	36.65	32.14	28.77	32.52
T³Former-O	3D-Occ	85.50	46.32	33.23	28.73	36.09	92.07	77.00	75.89	76.32	76.40
OccWorld-F [3, 48]	Camera	20.09	8.03	6.91	3.54	6.16	35.61	23.62	18.13	15.22	18.99
OccLLaMA-F [4, 48]	Camera	37.38	10.34	8.66	6.98	8.66	38.92	25.81	23.19	19.97	22.99
OccLLM-F [5, 48]	Camera	-	11.28	10.21	9.13	10.21	-	27.11	24.07	20.19	23.79
T³Former-F [48]	Camera	43.52	24.87	18.30	15.63	19.60	54.31	38.98	37.45	31.89	36.11

Table 1: Testing performance comparison with SOTA methods on the 4D occupancy forecasting task. Best values in each metric are **bolded**. 0s refers to reconstruction accuracy, while 1s, 2s, and 3s denote future prediction accuracy. Avg. is the average of 1s, 2s, and 3s.

cross-attention to predict the next action \hat{a}^{t+k+1} . The autoregressive generation of motion plans is defined as:

$$\hat{a}^{t+k+1} = \Phi_{\text{act}}(\hat{a}^{t+k-\tau_p:t+k}, \hat{s}^{t+k-1}, \Delta\hat{s}^{t+k}, Q_a^{t+k}). \quad (10)$$

Unlike OccWorld [3], we do not require an additional ego token to continuously track the agent’s motion trajectory. Instead, we can learn future motion directly from the scene changes and historical motion, as shown in Figure 3.

The optimization objective is defined as follows:

$$J_{\text{act}} = \mathbb{E}_{t,k}[\mathcal{L}_{\text{act}}(\hat{a}^{t+k}, a^{t+k})], \quad (11)$$

where \mathcal{L}_{act} measures the L2 discrepancy between the predicted and GT trajectories.

4 Experiments

4.1 Experimental settings

Targets and evaluation metrics. The main focus of OWM is jointly modeling occupancy forecasting and motion planning. Following the conventions in [3, 5, 4], we use the past four frames (2 seconds) to predict the outcomes of the next six frames (3 seconds). We conduct two sets of experiments:

- To validate the accuracy of 4D occupancy forecasting, we use intersection over union (IoU) and mean IoU (mIoU) across all semantic classes to measure the predicted future occupancy under the Occ3D dataset [17].
- To assess the precision and safety of motion planning, we calculate the L2 distance (in meters) between the planned and GT trajectories, and the collision rate with traffic participants’ bounding boxes using the nuScenes dataset [49].

Implementation details. The dataset consists of 1,000 scenes, of which 850 are used for training and 100 for testing. Each scene contains up to 40 timesteps, with a sampling frequency of 2Hz. The dimensions of the occupancy data S^t at each timestep are $16 \times 200 \times 200$. The pre-trained Triplane feature dimensions are $8 \times 16 \times 100 \times 100$. In Φ_{fut} , predictions for each plane incorporate features at $V = 5$ different scales, while the token dimension in Φ_{act} is $d_{\text{act}} = 50$. The objectives, $J_{\text{enc,dec}}$, J_{fut} , and J_{mot} , are optimized using AdamW with a weight regularization factor of 0.01, an initial learning rate of 0.001, and cosine decay with a minimum learning rate of 10^{-6} . We first pre-train Φ_{enc} and Φ_{dec} with a batch size of 10, using random flip augmentation to obtain the triplane representations. Then, we train Φ_{fut} and Φ_{act} with a batch size of 1, while fine-tuning Φ_{dec} . All training and testing are performed on 4 RTX 4090 GPUs. More details are provided in the supplementary material.

4.2 Comparisons with the state-of-the-art

4.2.1 4D occupancy forecasting

Table 1 presents the performance results of various methods, considering two modes of operation: (i) using 3D occupancy GTs as historical input, marked with “-O”; (ii) using predicted 3D occupancy data from FB-Occ [48] as

Models	Input	Auxiliary supervision	L2 (m) ↓				Collision rate (%) ↓			
			1s	2s	3s	Avg.	1s	2s	3s	Avg.
IL [50]	LiDAR	None	0.44	1.15	2.47	1.35	0.08	0.27	1.95	0.77
NMP [51]	LiDAR	Box+Motion	0.53	1.25	2.67	1.48	0.04	<u>0.12</u>	0.87	0.34
FF [52]	LiDAR	Freespace	0.55	1.20	2.54	1.43	0.06	0.17	1.07	0.43
EO [53]	LiDAR	Freespace	0.67	1.36	2.78	1.60	0.04	0.09	0.88	0.33
ST-P3 [8]	Camera	Map+Box+Depth	1.33	2.11	2.90	2.11	0.23	0.62	1.27	0.71
UniAD [6]	Camera	Map+Box+Motion+Track+Occ	0.48	<u>0.96</u>	1.65	<u>1.03</u>	<u>0.05</u>	0.17	<u>0.71</u>	<u>0.31</u>
VAD [7]	Camera	Map+Box+Motion	0.54	1.15	1.98	1.22	0.04	0.39	1.17	0.53
OccNet [15]	Camera	Map+Box+3D-Occ	1.29	2.13	2.99	2.14	0.21	0.59	1.37	0.72
OccNet [15]	3D-Occ	Map+Box	1.29	2.31	2.98	2.25	0.20	0.56	1.30	0.69
OccWorld-O [3]	3D-Occ	None	0.43	1.08	1.99	1.17	<u>0.07</u>	0.38	1.35	0.60
OccLLaMA-O [4]	3D-Occ	None	<u>0.37</u>	1.02	2.03	1.14	0.04	0.24	1.20	0.49
T ³ Former-O	3D-Occ	None	0.32	0.91	<u>1.76</u>	1.00	0.08	0.32	0.51	0.30

Table 2: Testing performance of motion planning compared with SOTA method. Best and second-best values in each metric are **bolded** and underlined, respectively. Auxiliary supervision refers to additional supervision signals beyond the GT trajectories.

historical input, marked with “-F”. “Copy&Paste” refers to directly using the GT occupancy data from the current timestep as predictions for future outcomes. Vanilla-LLaMA-O refers to the method that simply flattens the occupancy data and feeds it into LLaMA [54] for training.

It is clear that SOTA methods’ Φ_{enc} fail to achieve high-fidelity compression, resulting in low reconstruction accuracy at time 0s. In contrast, both T³Former-O and T³Former-F utilize triplane representations that preserve both geometric and semantic information, leading to the highest mIoU and IoU reconstruction accuracy. This significantly aids in Φ_{fit} for predicting the next 3 seconds, effectively reducing error accumulation. Specifically, the “Copy&Paste” method, as a simple baseline, demonstrates substantial error accumulation. In contrast, T³Former-O shows a significant reduction in error, as indicated by mIoU and IoU averages. Notably, IoU generally surpasses mIoU, as predicting occupancy (whether occupied or unoccupied) is relatively straightforward, while semantic tracking without instance-level supervision is more challenging and prone to drift over time.

4.2.2 Motion planning

We extensively compare T³Former with SOTA methods for autonomous driving, including LiDAR-based methods (IL [50], NMP [51], FF [52], and EO [53]), camera-based methods (ST-P3 [8], UniAD [6], VAD [7], and OccNet [15]), and occupancy-based methods (OccNet [15], OccWorld [3], and OccLLaMA [4]). LiDAR- and camera-based methods explore various combinations of auxiliary supervisions to enhance the quality of planned motion trajectories. Despite their success, the auxiliary information they rely on is labor-intensive to obtain.

In contrast, occupancy-based methods generate motion proposals using only occupancy representations. T³Former achieves the lowest L2 error over time, the lowest collision rate at the final time step, and the lowest average collision rate across all future motions. Compared to SOTA occupancy-based methods, T³Former reduces the average L2 error by 12.3% and the average collision rate by 38.8%. This is primarily because T³Former can establish precise, task-relevant correlations between scene changes and motion trajectories in a deep latent space, effectively filtering out noise from scene variations.

4.3 Visualizations

Comparisons with SOTA. Figure 4 illustrates the evolution of the scene over the next 3 seconds, along with the corresponding motion predictions for two different scenarios. (i) In the first case, it is clear that OccWorld-O incorrectly labels the truck as a trailer initially, resulting in a continuous accumulation of errors. In contrast, T³Former effectively learns the motion dynamics of all objects in the scene, consistently tracking each vehicle over a long horizon, while providing clearer object boundaries. (ii) In the second case, as the prediction horizon extends, OccWorld-O’s road boundary gradually fades, losing its clarity, whereas our method maintains the boundary shape of the road, including the trees. Additionally, OccWorld-O misidentifies the motorcycle as a truck at both 2.5s and 3s, while T³Former-O ensures that the semantics of small objects remain accurate over time. (iii) Under both scenarios, T³Former-O enables

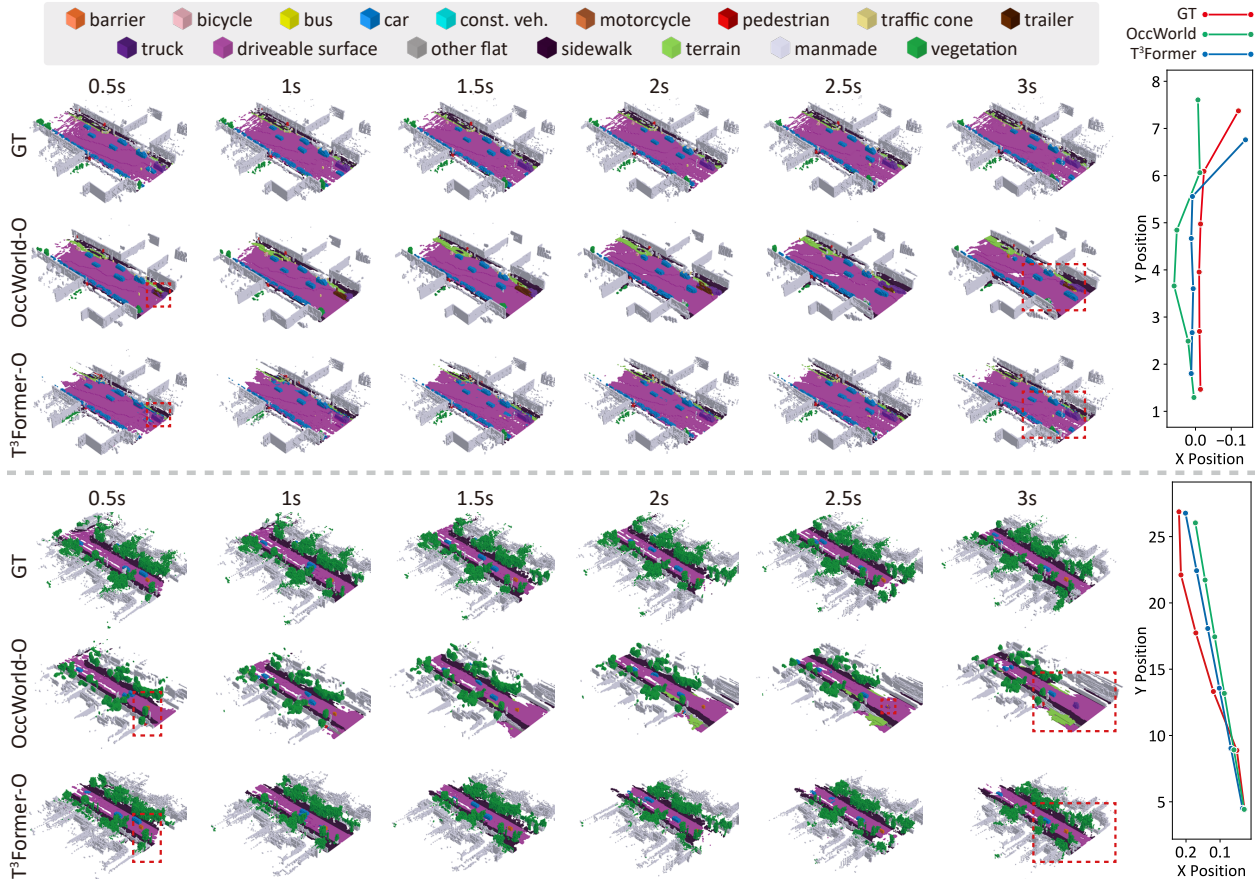


Figure 4: Visualization of 4D occupancy forecasting and motion planning for the next 3 seconds (zoom in for a clearer view).

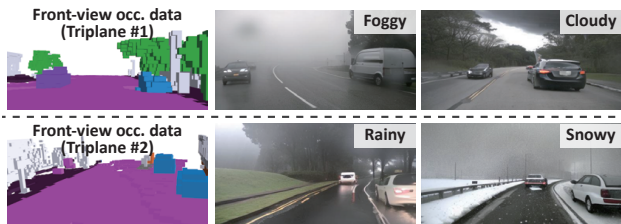


Figure 5: Driving view generations conditioned on different weather prompts and different triplane constraints.

precise long-term future predictions, allowing our motion planning to rely solely on the evolving scene dynamics. This leads to more accurate trajectories and better avoidance of potential future hazards.

Driving view generation. Recent diffusion-based autonomous driving models [12, 13, 11] typically use historical driving views as conditions to generate future views. In contrast, our approach uses only triplane data as a lightweight condition. We fine-tune the diffusion model with ControlNet [55]. Figure 5 showcases synthetic images generated with different weather prompts and different triplane conditions. Triplane provides accurate 3D structural information, thereby enhancing consistency between pixel positions and semantics in the resulting synthetic 2D images.

Comparison of motion prediction. Figure 6 compares occupancy predictions for the three furthest frames in the prediction window, focusing on dynamic objects of varying sizes (cars and pedestrians) from a BEV perspective. Two reference lines are displayed to reflect the errors between the predictions and GT. The results of our method match the GT significantly better than OccWorld-O, which exhibits substantial drift. For instance, the predictions for the pedestrians at the top and the vehicle on the left clearly demonstrate this improvement

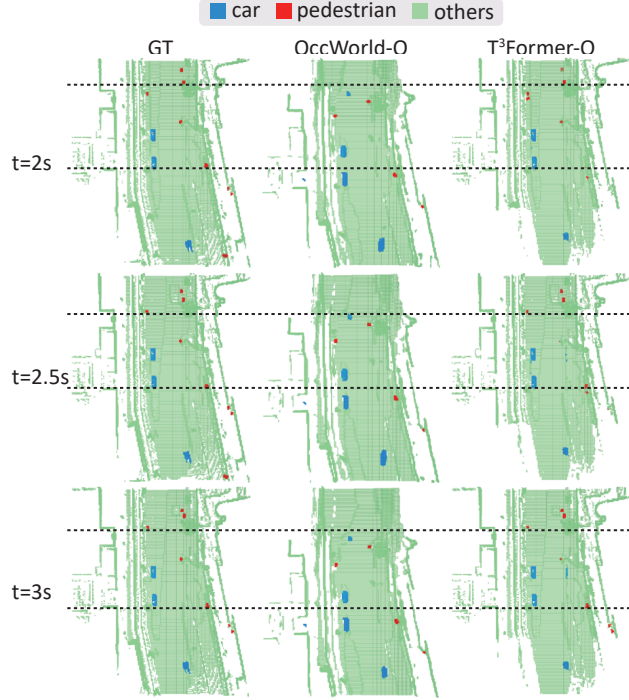


Figure 6: Predicted locations of dynamic objects for the three last frames in the prediction window.

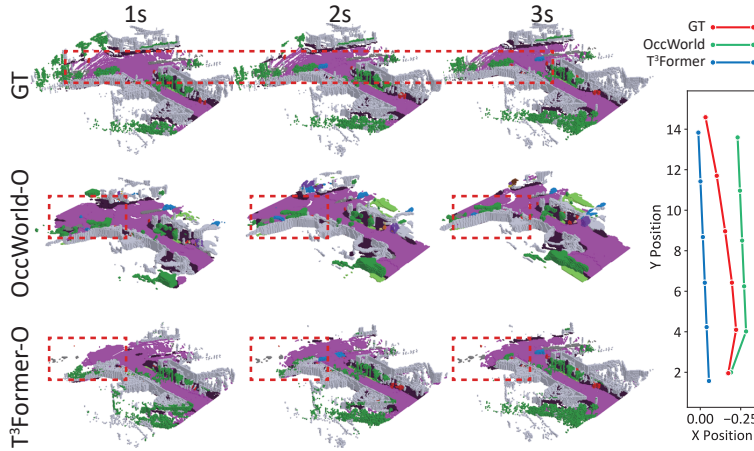


Figure 7: A failure case at a T-junction scenario.

Failure case. Figure 7 shows a failure case across three frames, where the road boundary at the end contains sparse occupied voxels, making the prediction challenging. Due to the inherent blurring issue of VAE [56, 57], OccWorld predictions tend to smooth and homogenize the sparse regions. In contrast, the triplane consists of fine-grained geometric details, which causes our predictions to also exhibit sparse boundaries, resulting in some deviation in the trajectory.

4.4 Ablation study

To validate the effectiveness of the key designs in T³Former, we conduct ablation studies by evaluating the averaged mIoU and averaged L2 across future outcomes, as shown in Table 3. **M0** represents our complete version. For fairness, all ablation models are derived by replacing specific modules in **M0**, as outlined below: **M1** replaces the input of T³Former with the VQ-VAE token from OccWorld [3], which results in a significant performance drop. **M2** uses a single-scale Transformer to learn temporal dynamics based on triplane representations, which fails to capture the

motion patterns of multi-scale objects, leading to poor performance. **M3** leverages multi-scale Transformers for parallel forecasting, as shown in Figure 1a, instead of autoregression, which leads to error accumulation. **M4** directly predicts the entire future triplane, demonstrating that predicting changes in the triplane is more efficient.

Idx.	Models	Avg. mIoU \uparrow	Avg. L2 \downarrow
M0	T ³ Former-O	34.70	0.63
M1	w/o Triplane	25.76	0.96
M2	w/o Multi-scale mot.	31.92	0.87
M3	w/o Autoregression	32.44	0.79
M4	w/o Changing triplane	33.81	0.71

Table 3: Ablation study of the components in T³Former.

4.5 Efficiency analysis

The predefined latent space shapes of OccWorld [3] and OccLLM [5] are $128 \times 50 \times 50$ and $64 \times 50 \times 50$, respectively. In contrast, T³Former only requires a compact triplane representation that is in spirit similar to orthogonal decomposition [33, 32]. Specifically, the xy plane has a shape of $8 \times 100 \times 100$, while the xz and yz planes are represented with shapes of $8 \times 100 \times 16$. This results in the smallest latent shape and parameter count for $\Phi_{\text{enc,dec}}$, while achieving superior reconstruction accuracy, as shown in Table 4.

Models	Latent shape \downarrow	Params (M) \downarrow	Reconstruction	
			mIoU \uparrow	IoU \uparrow
OccWorld [3]	320,000	14.17	60.50	59.07
OccLLM [5]	160,000	2.30	71.08	62.74
T³Former	105,600	0.69	85.50	92.07

Table 4: Comparisons of latent representations within OWMs.

Based on the triplane representation learned by Φ_{enc} , our Φ_{fut} only needs to learn the changes in the triplane, while Φ_{act} predicts the motion trajectory based on these changes. This results in our lightweight design, with a total parameter count of 55M, compared to OccWorld’s 72M, achieving a 23% reduction. As shown in Figure 1c, T³Former achieves 26 FPS for predicting each future frame on an RTX 4090 GPU, whereas OccWorld delivers only 18 FPS.

5 Conclusion

This paper proposes a new 4D occupancy world model, T³Former, which features three key designs: (i) pre-training triplane representations for OWM, (ii) capturing comprehensive motion dynamics using multi-scale Transformers, and (iii) predicting triplane changes for occupancy forecasting and motion planning. T³Former achieves SOTA performance in 4D occupancy forecasting and motion planning, with real-time capability. Our future work will dive deeper into the generation of driving views, as shown in Figure 5, focusing on the synergy between prompt constraints, image texture, and T³Former.

References

- [1] David Ha and Jürgen Schmidhuber. World models. *arXiv preprint arXiv:1803.10122*, 2018.
- [2] David Ha and Jürgen Schmidhuber. Recurrent world models facilitate policy evolution. *Advances in neural information processing systems*, 31, 2018.
- [3] Wenzhao Zheng, Weiliang Chen, Yuanhui Huang, Borui Zhang, Yueqi Duan, and Jiwen Lu. Occworld: Learning a 3d occupancy world model for autonomous driving. In *European conference on computer vision*, pages 55–72. Springer, 2024.
- [4] Julong Wei, Shanshuai Yuan, Pengfei Li, Qingda Hu, Zhongxue Gan, and Wenchao Ding. Occllama: An occupancy-language-action generative world model for autonomous driving. *arXiv preprint arXiv:2409.03272*, 2024.

- [5] Tianshuo Xu, Hao Lu, Xu Yan, Yingjie Cai, Bingbing Liu, and Yingcong Chen. Occ-llm: Enhancing autonomous driving with occupancy-based large language models. In *International Conference on Robotics and Automation*, 2025.
- [6] Yihan Hu, Jiazhi Yang, Li Chen, Keyu Li, Chonghao Sima, Xizhou Zhu, Siqi Chai, Senyao Du, Tianwei Lin, Wenhai Wang, et al. Planning-oriented autonomous driving. In *Proceedings of the IEEE/CVF conference on computer vision and pattern recognition*, pages 17853–17862, 2023.
- [7] Bo Jiang, Shaoyu Chen, Qing Xu, Bencheng Liao, Jiajie Chen, Helong Zhou, Qian Zhang, Wenyu Liu, Chang Huang, and Xinggong Wang. Vad: Vectorized scene representation for efficient autonomous driving. In *Proceedings of the IEEE/CVF International Conference on Computer Vision*, pages 8340–8350, 2023.
- [8] Shengchao Hu, Li Chen, Penghao Wu, Hongyang Li, Junchi Yan, and Dacheng Tao. St-p3: End-to-end vision-based autonomous driving via spatial-temporal feature learning. In *European Conference on Computer Vision*, pages 533–549. Springer, 2022.
- [9] Yumeng Zhang, Shi Gong, Kaixin Xiong, Xiaoqing Ye, Xiao Tan, Fan Wang, Jizhou Huang, Hua Wu, and Haifeng Wang. Bevworld: A multimodal world model for autonomous driving via unified bev latent space. *arXiv preprint arXiv:2407.05679*, 2024.
- [10] Zehuan Wu, Jingcheng Ni, Xiaodong Wang, Yuxin Guo, Rui Chen, Lewei Lu, Jifeng Dai, and Yuwen Xiong. Holodrive: Holistic 2d-3d multi-modal street scene generation for autonomous driving. *arXiv preprint arXiv:2412.01407*, 2024.
- [11] Yuqi Wang, Jiawei He, Lue Fan, Hongxin Li, Yuntao Chen, and Zhaoxiang Zhang. Driving into the future: Multiview visual forecasting and planning with world model for autonomous driving. In *Proceedings of the IEEE/CVF Conference on Computer Vision and Pattern Recognition*, pages 14749–14759, 2024.
- [12] Xiaofeng Wang, Zheng Zhu, Guan Huang, Xinze Chen, Jiagang Zhu, and Jiwen Lu. Drivedreamer: Towards real-world-drive world models for autonomous driving. In *European Conference on Computer Vision*, pages 55–72. Springer, 2024.
- [13] Shenyuan Gao, Jiazhi Yang, Li Chen, Kashyap Chitta, Yihang Qiu, Andreas Geiger, Jun Zhang, and Hongyang Li. Vista: A generalizable driving world model with high fidelity and versatile controllability. *Advances in Neural Information Processing Systems*, 37:91560–91596, 2025.
- [14] Fan Jia, Weixin Mao, Yingfei Liu, Yucheng Zhao, Yuqing Wen, Chi Zhang, Xiangyu Zhang, and Tiancai Wang. Adriver-i: A general world model for autonomous driving. *arXiv preprint arXiv:2311.13549*, 2023.
- [15] Wenwen Tong, Chonghao Sima, Tai Wang, Li Chen, Silei Wu, Hanming Deng, Yi Gu, Lewei Lu, Ping Luo, Dahua Lin, et al. Scene as occupancy. In *Proceedings of the IEEE/CVF International Conference on Computer Vision*, pages 8406–8415, 2023.
- [16] Qihang Ma, Xin Tan, Yanyun Qu, Lizhuang Ma, Zhizhong Zhang, and Yuan Xie. Cotr: Compact occupancy transformer for vision-based 3d occupancy prediction. In *Proceedings of the IEEE/CVF Conference on Computer Vision and Pattern Recognition*, pages 19936–19945, 2024.
- [17] Xiaoyu Tian, Tao Jiang, Longfei Yun, Yucheng Mao, Huitong Yang, Yue Wang, Yilun Wang, and Hang Zhao. Occ3d: A large-scale 3d occupancy prediction benchmark for autonomous driving. *Advances in Neural Information Processing Systems*, 36:64318–64330, 2023.
- [18] Yi Wei, Linqing Zhao, Wenzhao Zheng, Zheng Zhu, Jie Zhou, and Jiwen Lu. Surroundocc: Multi-camera 3d occupancy prediction for autonomous driving. In *Proceedings of the IEEE/CVF International Conference on Computer Vision*, pages 21729–21740, 2023.
- [19] Rui Liu, Wenguan Wang, and Yi Yang. Volumetric environment representation for vision-language navigation. In *Proceedings of the IEEE/CVF Conference on Computer Vision and Pattern Recognition*, pages 16317–16328, 2024.
- [20] Tesla ai day. (2021).
- [21] Junyi Ma, Xieyuanli Chen, Jiawei Huang, Jingyi Xu, Zhen Luo, Jintao Xu, Weihao Gu, Rui Ai, and Hesheng Wang. Cam4docc: Benchmark for camera-only 4d occupancy forecasting in autonomous driving applications. In *Proceedings of the IEEE/CVF Conference on Computer Vision and Pattern Recognition*, pages 21486–21495, 2024.
- [22] Aaron Van Den Oord, Oriol Vinyals, et al. Neural discrete representation learning. *Advances in neural information processing systems*, 30, 2017.
- [23] Ali Razavi, Aaron Van den Oord, and Oriol Vinyals. Generating diverse high-fidelity images with vq-vae-2. *Advances in neural information processing systems*, 32, 2019.

- [24] Yuming Jiang, Shuai Yang, Tong Liang Koh, Wayne Wu, Chen Change Loy, and Ziwei Liu. Text2performer: Text-driven human video generation. In *Proceedings of the IEEE/CVF International Conference on Computer Vision*, pages 22747–22757, 2023.
- [25] Hang Zhang, Anton Savov, and Benjamin Dillenburger. Maskplan: Masked generative layout planning from partial input. In *Proceedings of the IEEE/CVF Conference on Computer Vision and Pattern Recognition*, pages 8964–8973, 2024.
- [26] Jiabao Wang, Zhaojiang Liu, Qiang Meng, Liujiang Yan, Ke Wang, Jie Yang, Wei Liu, Qibin Hou, and Ming-Ming Cheng. Opus: occupancy prediction using a sparse set. *arXiv preprint arXiv:2409.09350*, 2024.
- [27] Ashish Vaswani, Noam Shazeer, Niki Parmar, Jakob Uszkoreit, Llion Jones, Aidan N Gomez, Łukasz Kaiser, and Illia Polosukhin. Attention is all you need. *Advances in neural information processing systems*, 30, 2017.
- [28] Rajaei Khatib and Raja Giryes. Trinerflet: A wavelet based triplane nerf representation. In *European Conference on Computer Vision*, pages 358–374. Springer, 2024.
- [29] J Ryan Shue, Eric Ryan Chan, Ryan Po, Zachary Ankner, Jiajun Wu, and Gordon Wetzstein. 3d neural field generation using triplane diffusion. In *Proceedings of the IEEE/CVF Conference on Computer Vision and Pattern Recognition*, pages 20875–20886, 2023.
- [30] Tao Hu, Xiaogang Xu, Ruihang Chu, and Jiaya Jia. Trivol: Point cloud rendering via triple volumes. In *Proceedings of the IEEE/CVF Conference on Computer Vision and Pattern Recognition*, pages 20732–20741, 2023.
- [31] Luchuan Song, Pinxin Liu, Lele Chen, Guojun Yin, and Chenliang Xu. Tri 2-plane: Thinking head avatar via feature pyramid. In *European Conference on Computer Vision*, pages 1–20. Springer, 2024.
- [32] Yuanhui Huang, Wenzhao Zheng, Yunpeng Zhang, Jie Zhou, and Jiwen Lu. Tri-perspective view for vision-based 3d semantic occupancy prediction. In *Proceedings of the IEEE/CVF conference on computer vision and pattern recognition*, pages 9223–9232, 2023.
- [33] Jumin Lee, Sebin Lee, Changho Jo, Woobin Im, Juhyeong Seon, and Sung-Eui Yoon. Semcity: Semantic scene generation with triplane diffusion. In *Proceedings of the IEEE/CVF conference on computer vision and pattern recognition*, pages 28337–28347, 2024.
- [34] Xu Yan, Jiantao Gao, Jie Li, Ruimao Zhang, Zhen Li, Rui Huang, and Shuguang Cui. Sparse single sweep lidar point cloud segmentation via learning contextual shape priors from scene completion. In *Proceedings of the AAAI conference on artificial intelligence*, volume 35, pages 3101–3109, 2021.
- [35] Jinke Li, Xiao He, Chonghua Zhou, Xiaoqiang Cheng, Yang Wen, and Dan Zhang. Viewformer: Exploring spatiotemporal modeling for multi-view 3d occupancy perception via view-guided transformers. In *European Conference on Computer Vision*, pages 90–106. Springer, 2024.
- [36] Fan Lu, Guang Chen, Zhijun Li, Lijun Zhang, Yinlong Liu, Sanqing Qu, and Alois Knoll. Monet: Motion-based point cloud prediction network. *IEEE Transactions on Intelligent Transportation Systems*, 23(8):13794–13804, 2021.
- [37] Benedikt Mersch, Xieyuanli Chen, Jens Behley, and Cyrill Stachniss. Self-supervised point cloud prediction using 3d spatio-temporal convolutional networks. In *Conference on Robot Learning*, pages 1444–1454. PMLR, 2022.
- [38] Tarasha Khurana, Peiyun Hu, David Held, and Deva Ramanan. Point cloud forecasting as a proxy for 4d occupancy forecasting. In *Proceedings of the IEEE/CVF Conference on Computer Vision and Pattern Recognition*, pages 1116–1124, 2023.
- [39] Junliang Chen, Huaiyuan Xu, Yi Wang, and Lap-Pui Chau. Occprophet: Pushing efficiency frontier of camera-only 4d occupancy forecasting with observer-forecaster-refiner framework. In *ICLR*, 2025.
- [40] Jingyi Xu, Xieyuanli Chen, Junyi Ma, Jiawei Huang, Jintao Xu, Yue Wang, and Ling Pei. Spatiotemporal decoupling for efficient vision-based occupancy forecasting. *arXiv preprint arXiv:2411.14169*, 2024.
- [41] Haoran Xu, Peixi Peng, Xinyi Zhang, Guang Tan, Yaokun Li, Shuaixian Wang, and Luntong Li. Exploiting continuous motion clues for vision-based occupancy prediction. In *AAAI*, 2025.
- [42] Maxim Berman, Amal Rannen Triki, and Matthew B Blaschko. The lovasz-softmax loss: A tractable surrogate for the optimization of the intersection-over-union measure in neural networks. In *Proceedings of the IEEE conference on computer vision and pattern recognition*, pages 4413–4421, 2018.
- [43] Tom Brown, Benjamin Mann, Nick Ryder, Melanie Subbiah, Jared D Kaplan, Prafulla Dhariwal, Arvind Nee-lakantan, Pranav Shyam, Girish Sastry, Amanda Askell, et al. Language models are few-shot learners. *Advances in neural information processing systems*, 33:1877–1901, 2020.

- [44] Shaoyu Liu, Jianing Li, Guanghui Zhao, Yunjian Zhang, Xin Meng, Fei Richard Yu, Xiangyang Ji, and Ming Li. Eventgpt: Event stream understanding with multimodal large language models. *arXiv preprint arXiv:2412.00832*, 2024.
- [45] Gengze Zhou, Yicong Hong, and Qi Wu. Navgpt: Explicit reasoning in vision-and-language navigation with large language models. In *Proceedings of the AAAI Conference on Artificial Intelligence*, volume 38, pages 7641–7649, 2024.
- [46] Olaf Ronneberger, Philipp Fischer, and Thomas Brox. U-net: Convolutional networks for biomedical image segmentation. In *Medical image computing and computer-assisted intervention–MICCAI 2015: 18th international conference, Munich, Germany, October 5-9, 2015, proceedings, part III 18*, pages 234–241. Springer, 2015.
- [47] Kaiming He, Xiangyu Zhang, Shaoqing Ren, and Jian Sun. Deep residual learning for image recognition. In *Proceedings of the IEEE conference on computer vision and pattern recognition*, pages 770–778, 2016.
- [48] Zhiqi Li, Zhiding Yu, David Austin, Mingsheng Fang, Shiyi Lan, Jan Kautz, and Jose M Alvarez. FB-OCC: 3D occupancy prediction based on forward-backward view transformation. *arXiv:2307.01492*, 2023.
- [49] Holger Caesar, Varun Bankiti, Alex H Lang, Sourabh Vora, Venice Erin Liong, Qiang Xu, Anush Krishnan, Yu Pan, Giancarlo Baldan, and Oscar Beijbom. nuscenes: A multimodal dataset for autonomous driving. In *Proceedings of the IEEE/CVF conference on computer vision and pattern recognition*, pages 11621–11631, 2020.
- [50] Nathan D Ratliff, J Andrew Bagnell, and Martin A Zinkevich. Maximum margin planning. In *Proceedings of the 23rd international conference on Machine learning*, pages 729–736, 2006.
- [51] Wenyuan Zeng, Wenjie Luo, Simon Suo, Abbas Sadat, Bin Yang, Sergio Casas, and Raquel Urtasun. End-to-end interpretable neural motion planner. In *Proceedings of the IEEE/CVF conference on computer vision and pattern recognition*, pages 8660–8669, 2019.
- [52] Peiyun Hu, Aaron Huang, John Dolan, David Held, and Deva Ramanan. Safe local motion planning with self-supervised freespace forecasting. In *Proceedings of the IEEE/CVF Conference on Computer Vision and Pattern Recognition*, pages 12732–12741, 2021.
- [53] Tarasha Khurana, Peiyun Hu, Achal Dave, Jason Ziglar, David Held, and Deva Ramanan. Differentiable raycasting for self-supervised occupancy forecasting. In *European Conference on Computer Vision*, pages 353–369. Springer, 2022.
- [54] Hugo Touvron, Thibaut Lavril, Gautier Izacard, Xavier Martinet, Marie-Anne Lachaux, Timothée Lacroix, Baptiste Rozière, Naman Goyal, Eric Hambro, Faisal Azhar, et al. Llama: Open and efficient foundation language models. *arXiv preprint arXiv:2302.13971*, 2023.
- [55] Lvmin Zhang, Anyi Rao, and Maneesh Agrawala. Adding conditional control to text-to-image diffusion models. In *Proceedings of the IEEE/CVF international conference on computer vision*, pages 3836–3847, 2023.
- [56] Dooseop Choi and KyoungWook Min. Hierarchical latent structure for multi-modal vehicle trajectory forecasting. In *European conference on computer vision*, pages 129–145. Springer, 2022.
- [57] Irina Higgins, Loic Matthey, Arka Pal, Christopher Burgess, Xavier Glorot, Matthew Botvinick, Shakir Mohamed, and Alexander Lerchner. beta-vae: Learning basic visual concepts with a constrained variational framework. In *International conference on learning representations*, 2017.